Spin wave modes in ferromagnetic tubes

A. Kozhanov, M. Popov, I. Zavislyak, D. Ouellette, D. W. Lee et al.

Citation: J. Appl. Phys. **111**, 013905 (2012); doi: 10.1063/1.3672835
View online: http://dx.doi.org/10.1063/1.3672835
View Table of Contents: http://jap.aip.org/resource/1/JAPIAU/v111/i1
Published by the American Institute of Physics.

Spin wave modes in ferromagnetic tubes

A. Kozhanov,[1,a)] M. Popov,[2] I. Zavislyak,[2] D. Ouellette,[1] D. W. Lee,[3] S. X. Wang,[3] M. Rodwell,[1] and S. J. Allen[1]
[1]*University of California at Santa Barbara, Santa Barbara, California 93106, USA*
[2]*Taras Shevchenko National University of Kyiv 64, Volodymyrs'ka St., 01601 Kyiv, Ukraine*
[3]*Department of Materials Science and Engineering, Stanford University, Stanford, California 94305, USA*

(Received 10 August 2011; accepted 29 November 2011; published online 4 January 2012)

Resonances are observed in the transmission between two coplanar waveguides coupled by ferromagnetic $Co_{90}Ta_5Zr_5$ tubes that wrap around their shorted ends. The resonances are assigned to the magnetostatic surface waves that counter propagate along the tube perimeter. We use a model based on an infinite ferromagnetic tube, with elliptical cross section of roughly the same dimensions as the studied structure. Additional theoretical analysis of the fundamental precession mode observed in experiment is carried out. Periodic boundary conditions dictated by the tube perimeter and applied to magnetostatic surface waves quantitatively account for the experimentally observed bandwidth of excited modes, despite the contorted tubular shape. The tubular topology appears to be more important than the shape details. © *2012 American Institute of Physics*. [doi:10.1063/1.3672835]

I. INTRODUCTION

Potential applications in magnetic memory, sensors, signal processing and logic devices[1–8] has stimulated exploration of spin dynamics in microstructured ferromagnetic materials. Microwave devices based on magnetostatic spin waves in insulating ferrimagnetic materials like yttrium-iron garnet (YIG)[9] have long been explored and developed. However, future micro- and nanoscale spin wave based devices may benefit from exploiting ferromagnetic metals that are more easily deposited, processed and nanofabricated with advanced fabrication techniques than ferrimagnetic oxides. Further, ferromagnetic metals like CoTaZr, CoFe, and CoFeB have nearly an order of magnitude larger saturation magnetization than typical ferrimagnets.[10] As a result, they support higher and broader bands of spin wave resonances. Among the metallic ferromagnetic materials CoTaZr exhibits the lowest coercive fields of 2–10 Oe which enables using the shape anisotropy for self-alignment of the magnetization in the patterned ferromagnetic structures.

Lithographically patterned ferromagnetic films support shape defined magnetostatic spin wave modes quantized by the structure dimensions. Stripes and wires of various geometries, magnetic dots and antidot arrays have been intensively studied. Quantized spin wave modes,[11,12] spin wave "tunneling,"[13–16] current induced Doppler shifts,[17] nonreciprocal spin wave propagation,[18] magnon Bose-Einstein condensation[19] and various nonlinear effects[20,21] have been observed in these structures. Fabrication challenges have limited the number of experiments on magnetization dynamics in three dimensional geometries. Here, we describe the fabrication of ferromagnetic tubes coupled to coplanar waveguides, experimental investigation and theoretical modeling of their resonant excitations. Ferromagnetic tubes are potential building blocks for on-chip tunable microwave filters and transformers.

In this work we study quantized surface magnetostatic oscillations in micron sized ferromagnetic tubes formed by wrapping a metallic ferromagnetic film around exciting and detecting coupling loops at ends of coplanar waveguides. The ferromagnetic tube forms a closed magnetic circuit which traps the high frequency magnetic flux produced by the enclosed coupling loops. Analogous to the core in common transformers these tubes should efficiently, and resonantly, couple signals between coupling loops that share the same ferromagnetic tube. Resonances are displayed that are defined by the magnetostatic modes circulating on the inner and outer tube surfaces and indexed by periodic boundary conditions around the tubes despite their contorted geometry.

The magnetization ground state of tubular structures is strongly dependent on the tube length l and external and internal radii R and r.[22,23] Long and narrow tubes with $l \gg R$ form a simple ferromagnetic ground state with magnetic moments aligned along the tube axis. The opposite case, $R \gg l$, has the shape of a ring and supports a vortex state with tangential magnetization circling around the ring. Magnetization in short ferromagnetic tubes, or thick rings, can be found in either a vortex configuration or so-called "onion" state with two head to head vortex domains.

Recent theoretical[24–26] and experimental[23,27,28] work has focused on the magnetization dynamics in long ferromagnetic tubes magnetized along the tube axis. Theoretical models predict that resonances correspond to magnetostatic surface waves circulating around the tube and subject to periodic boundary conditions.[25,26] The experiments of Mendach *et al*. observed the spatially uniform ferromagnetic resonance in a Permalloy tube.[28] They did not report on the rich spectrum of magnetostatic spin waves that circulate around the tube. Demokritov *et al*. experimentally simulated tube like resonances by artificially introducing periodic boundary conditions in a ferrite stripe by providing electrical feedback between the exciting and detecting loops.[29] The most striking results have been obtained by Balhorn *et al*. on "self-assembled," rolled up, ferromagnetic

a)Electronic mail: kozhanov@cnsi.ucsb.edu.

microtubes.[30] They observed spin wave resonances in the self-assembled, multilayered, ferromagnetic tube with a circular cross section. The self-assembled structure produces a simple test structure, but does not promise a method for integration into high frequency circuits.

II. EXPERIMENTAL APPROACH

The ferromagnetic tubes together with coplanar waveguide coupling loops were fabricated in the following manner. (See Fig. 1.) A 200 nm thick amorphous ferromagnetic $Co_{90}Ta_5Zr_5$ film was sputtered onto an oxidized Si substrate (SiO_2 thickness of 200 nm). A saturation magnetization of $M_s = 955$ emu/cm^3 and a coercive field $H_c \sim 2$ Oe and effective anisotropy field of $H_a \sim 20$ Oe were measured on the unpatterned $Co_{90}Ta_5Zr_5$ film using a vibrating sample magnetometer. More detailed information on the magnetic properties of sputtered $Co_{90}Ta_5Zr_5$ films used in our experiments can be found in the literature.[2,31,32] Using lithographic techniques, the film was selectively etched in the ICP dry etch system with chlorine based chemistry to define pairs of 6 μm $\times$ 10 μm rectangles. The longer side of the rectangle, which later defined the ferromagnetic tube length, was aligned parallel to the easy axis of the magnetic film. The patterned ferromagnetic film was then covered with a 100 nm thick insulating SiO_2 layer. 100 nm thick aluminum coupling loops were lithographically formed by short-circuiting the ends of a pair of coplanar waveguides positioned over the $Co_{90}Ta_5Zr_5$ rectangles. The structure was covered with another SiO_2 insulating layer, 200 nm thick. 1 μm $\times$ 10 μm holes were dry-etched down to the bottom magnetic layer to allow a subsequent, patterned, layer of $Co_{90}Ta_5Zr_5$ to complete the magnetic circuit. The completed process resulted in two coplanar waveguides with 1 μm wide shorted ends, separated by 1 μm but wrapped together by an electrically isolated $Co_{90}Ta_5Zr_5$ film (Fig. 1). The $Co_{90}Ta_5Zr_5$ film formed a 10 μm long ferromagnetic tube-like structure aligned along the ferromagnetic film easy axis. It had 200 nm thick top and bottom walls that overlapped by 1 μm at the tube sides to close the tube magnetic circuit.

The "tubes" thus formed are of course not circular but topologically equivalent to a cylinder and provide a closed magnetic circuit [Figs. 1(b) and 1(c)] that captures the magnetic fields produced by the high frequency currents flowing in the shorted ends of the coplanar waveguides. Focused ion beam etching exposes the cross section imaged in the SEM micrograph [Fig. 1(b)].

Transmission and reflection S-parameters were measured at room temperature using an Agilent 8720ES vector network analyzer (VNA) operating from 0.05 to 20 GHz. Standard load-reflect-match calibration using the GGB Industries CS-5 calibration substrate was carried out. This procedure placed the VNA reference planes to the tips of the infinity GSG probes used to contact the fabricated sample.

Only transmission S_{21}, the ratio of high frequency voltage at terminals 2 to the input high frequency voltage at terminals 1, is analyzed in the following discussion. The test devices were positioned on the narrow gap of a small electromagnet that provided magnetic field bias up to 1000 Oe aligned along the tube axis. By comparing the S-parameters at disparate bias magnetic fields, the magnetic field independent instrument response and electromagnetic coupling between measurement ports can be effectively removed to expose the S-parameters related to the magnetostatic mode coupling of exciting and detecting loops of the coplanar waveguides. No magnetostatic coupling was detected in this

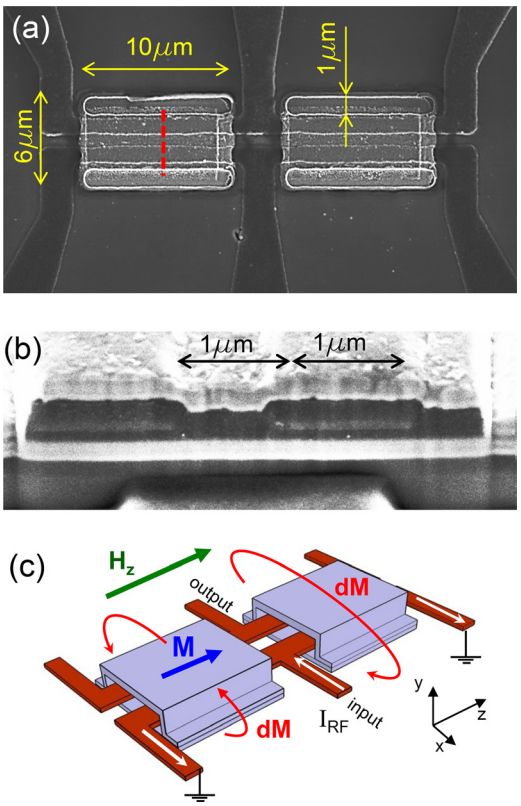

FIG. 1. (Color online) The shorted ends of two coplanar waveguides are coupled by a ferromagnetic "tube." Top view SEM (a) and SEM micrograph of structure cross section (b). Schematic of fabricated structure (c).

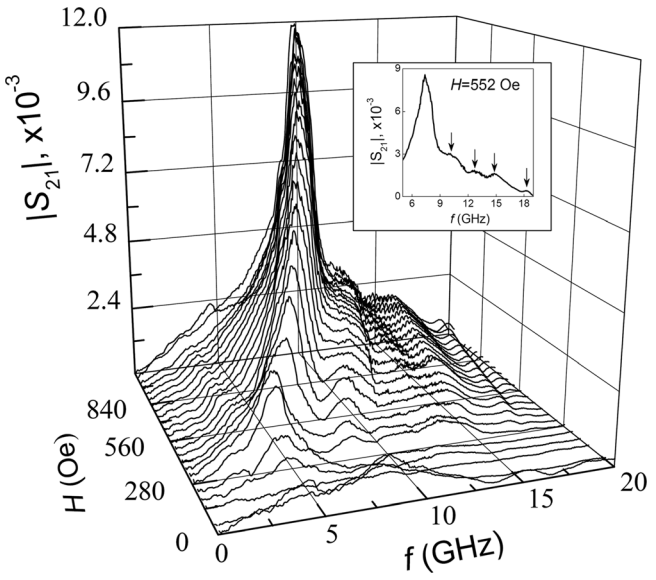

FIG. 2. Frequency and magnetic field dependence of $|S_{21}|$ measured with the fabricated structure. Insert: $|S_{21}|(f)$ measured at $H = 552$ Oe. Arrows indicate the peak positions.

device at bias magnetic fields of $H \sim 100$ Oe. The measurement at this magnetic field was used as a reference and subtracted from measurements at higher bias fields to remove the electromagnetic coupling.

III. RESULTS AND DISCUSSION

Results for $|S_{21}|(f,H)$ measured on the fabricated structure are shown in Fig. 2. At the low bias magnetic fields, $H_z < 200$ Oe, directed along the axis of the tube, $|S_{21}(f)|$ displayed a number of peaks, the frequency position of which was dependent on the history of the bias magnetic field. With increasing magnetic field bias from $H_z = 0$ Oe, the magnitude of these peaks decreases and related magnetic coupling disappears at $H_z \sim 100$ Oe. At $H_z \geq 200$ Oe we detect a strong peak followed by a series of smaller peaks. These peaks shift toward higher frequencies with increase of bias field, H_z. Transmission at the lowest frequency peak reaches $|S_{21}| \sim 0.012$ at $H_z = 988$ Oe.

The hysteretic low field behavior, $100 < H_z < 200$ Oe, is interpreted as follows. The closed magnetic circuit can effectively couple the two shorted ends of the coplanar waveguides only when the tube magnetization is predominantly oriented along the axis of the tubes, along the shorting lines of the coplanar waveguides. Only then can the microwave magnetic fields effectively induce changes in the magnetization and couple to the magnetostatic oscillations in the tubes. This condition occurs above 200 Oe. Below 200 Oe, the tube has multidomain structure that will produce some coupling, hysteretic in bias field and dependent on the bias field history.

This interpretation is supported by micromagnetic simulations[33] that investigate the magnetization alignment within our structures at magnetic field values $|H_z| \leq 2$ kOe. The tube geometry used in the micromagnetic simulations is schematically shown in insert in Fig. 3(a). The tube is formed by the 200 nm thick top and bottom magnetic layers, overlapping at the sides. The lateral dimensions of the model tube are the same as of the fabricated structure (Fig. 1). The following parameters were used in the simulation: $Co_{90}Ta_5Zr_5$ with $M_s = 955$ emu/cm^3, uniaxial anisotropy $K_{U2} = 1200$ erg/cm^3 with the easy axis aligned along the tube axis (Z direction), exchange stiffness $A = 1.050 \times 10^{-6}$ erg/cm^3, mesh size 1 nm.

The results of the simulations are shown in Fig. 3. At magnetic fields $H_z > 266$ Oe the majority of magnetic moments in the tube are aligned along the tube axis with some magnetic disorder at the tube ends. When the field is decreased the magnetization misalignment spreads toward the tube center and forms the domain wall in the middle of the tube. At $H = 0$ the magnetization alignment of the tube is described by a double vortex state.[22] The magnetization is mostly circularly oriented around the tube perimeter pointing in a clockwise direction on one end and counter-clock wise direction on the other end of the tube. This is similar to that was found by Lee *et al.* for circular ferromagnetic nanotubes.[23] Ferromagnetic magnetization alignment[22,23] of this tube cannot be achieved at $H = 0$ because the length of the tube is comparable to its other dimensions. As the field increases in the opposite direction the magnetization reorientation is achieved by forcing the vortices to either side as the center develops a uniform magnetization [Fig. 3(b)].

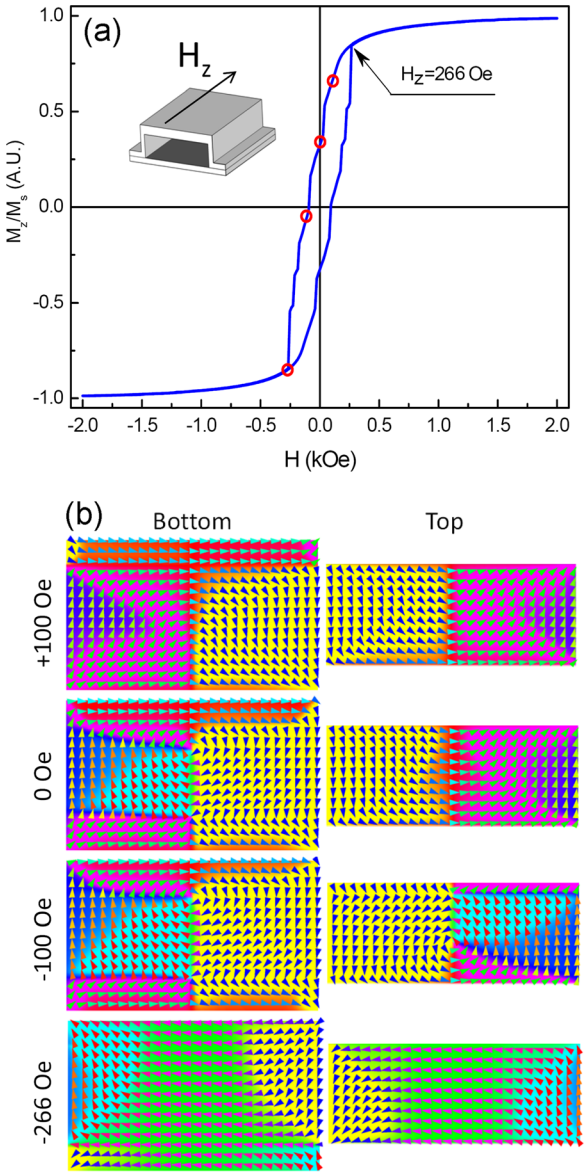

FIG. 3. (Color online) Results of micromagnetic simulations. Top: hysteresis curve, insert: tube model schematic; Bottom: schematic of magnetization alignment at various magnetic fields for the top and bottom walls of the tube.

The complex magnetic configuration of the tube at $|H_z| < 266$ Oe is dependent on the tube magnetization history. Most of the magnetic moments are not perpendicular to the exciting high frequency magnetic fields produced by the RF currents in the waveguide. The simulation suggests that this complex magnetic configuration is responsible for the low amplitude, bias history dependent, peaks in $|S_{21}(f)|$ measured at $H_z < 200$ Oe in our experiment.

At higher magnetic fields ($H_z > 266$ Oe) the magnetic moments are largely pointing along the tube axis. The high frequency magnetic field is perpendicular to the magnetic moments and can effectively excite the various magnetostatic magnetization oscillation modes. Starting from magnetic field values of ~200 Oe we detect a series of resonant peaks in $|S_{21}(f)|$ whose frequency increases with increasing H_z (Fig. 2). The development of the systematic reproducible structure above 200 Oe shown in Fig. 2 agrees with the

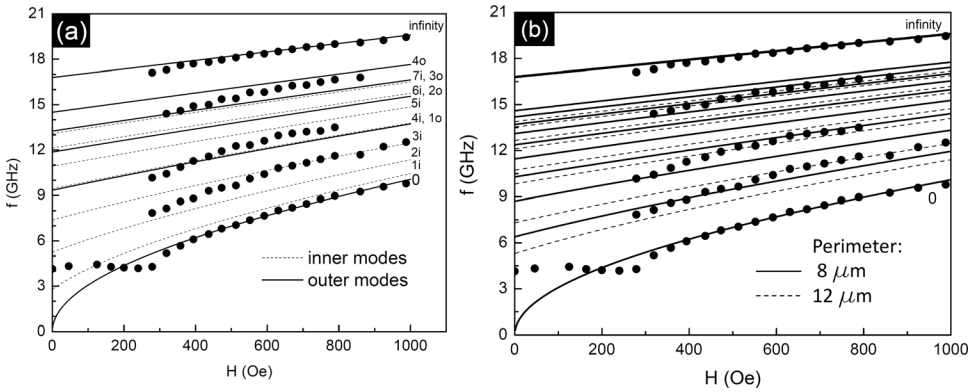

FIG. 4. Resonances in $|S_{21}|$ vs applied magnetic field. Experiment (circles). (a) Theory for tubes with elliptical profile (dashed lines — inner modes, solid lines —outer modes). Numbers indicate the outer (o) and inner (i) mode numbers.[26] (b) Theory for MSSW in infinite ferromagnetic film with periodic boundary conditions.[32] Solid lines — 12 μm perimeter, dashed lines — 8 μm perimeter.

results of the simulation: above 266 Oe, the magnetization of the tube is mostly aligned with the tube axis; the difference in the threshold magnetic fields can be attributed to the shape imperfections of the fabricated tube. The frequency position of the observed peaks in $|S_{21}(f)|$ and their shift with a magnetic field H_z are displayed in Fig. 4.

We used two theoretical models to analyze experimental results. First, we theoretically analyzed the experimental results using the model of the magnetostatic magnetization oscillations in the elliptical tube developed by Popov and Zavislyak.[26] According to their model the magnetostatic oscillations in the infinite tube with elliptical cross section are formed by a superposition of the two waves traveling in the opposite directions along the tube perimeter. The magnetization (and magnetic field) for these modes can be written in form $A_n e^{in\varphi} + B_n e^{-in\varphi}$, where A_n and B_n are the precession amplitudes and φ – elliptic cylindrical azimuthal coordinate, n – the mode number. In contrast to the magnetostatic waves in the tubes with circular cross section,[28] in elliptical tubes the wave amplitudes are not equal and both nonzero ($A_n \neq B_n$, A_n, $B_n \neq 0$) and the magnetostatic oscillation mode (except of $n=0$) can be expressed as a superposition of the traveling and standing magnetostatic waves: $A_n(e^{in\varphi} + e^{-in\varphi}) + (B_n - A_n)e^{-in\varphi}$. The energy fluxes of the waves traveling in the opposite directions cancel each other at some radial coordinate value within the wall of the tube. At the other radial coordinate values one of the energy fluxes dominates and forms a traveling wave with larger energy flux either on the inner or outer surfaces of the tube. Dispersion relation of these modes is given by the biquadratic equation:

$$(1+P)^2\omega^4 - s\omega^2 + q = 0, \tag{1}$$

where ω is the frequency of the magnetization oscillation,

$$s = 1/4\omega_M^2(1-r^{4n})(1-P)^2 + 2\omega_H(1+P)^2(\omega_M+\omega_H) + 2\omega_H^2 P(1-r^{2n}), \tag{2}$$

$$q = \left[\omega_H^2(1+P) + 1/2\omega_M^2(1-r^{2n}) + 1/2\omega_M\omega_H\left(r^{2n}(P-1) + P + 3\right)\right] \times \left[\omega_H^2(1+P) + 1/2\omega_M^2 P(1-r^{2n}) + 1/2\omega_M\omega_H\left(r^{2n}(1-P) + 3P + 1\right)\right],$$

$$P = \left(1-(c/2R_1)^{2n}\right)\Big/\left(1+(c/2R_1)^{2n}\right),$$

$$r = R_1/R_2, \quad R_1 = \frac{a_1+b_1}{2}, \quad R_2 = \frac{a_2+b_2}{2},$$

$\omega_H = \gamma H$, $\omega_M = \gamma 4\pi M_s$, γ is the gyromagnetic ratio, n is the mode number, and c is the semifocal length of the inner and outer ellipses. Equation (1) has two positive solutions which represent two families of spin wave modes in ferromagnetic tubes of elliptical profile:

$$\omega_n^{HF} = \frac{1}{1+P}\sqrt{1/2\left(s + \sqrt{s^2 - 4(1+P)^2 q}\right)}, \tag{3a}$$

$$\omega_n^{LF} = \frac{1}{1+P}\sqrt{1/2\left(s - \sqrt{s^2 - 4(1+P)^2 q}\right)}. \tag{3b}$$

The high frequency mode ω_n^{HF} has larger energy flux on the outer surface of the tube and the low frequency mode ω_n^{LF} has larger energy flux on the inner. For example, for $n=1$ mode the Pointing vector amplitudes on the inner and outer surfaces can be different by factor of 6 for certain geometries of the ellipsoid.[26]

We approximate the fabricated tube with an elliptical tube with the following dimensions: $a_1 = 1.899\ \mu$m, $a_2 = 1.925\ \mu$m, $b_2 = 0.350\ \mu$m, $b_1 = 0.150\ \mu$m. The cross section of the fabricated tube is shown in Fig. 5 and compared with the aforementioned elliptical tube. The inner and outer ellipses are confocal. Results of approximation are shown as lines in Fig. 4(a). At $H > 200$ Oe the mode with $n=0$ fits well the strongest (lowest frequency) peak observed in the experiment.

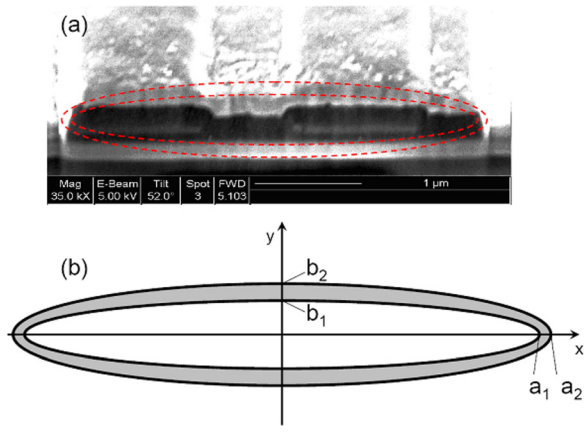

FIG. 5. (Color online) SEM image of the fabricated ferromagnetic tube cross section (a) and schematic of model elliptical tube cross section (b).

Additional theoretical analysis of the $n = 0$ mode was carried out. Following the Popov-Zavislyak model[26] and their notation we can directly solve Maxwell equations in the magnetostatic limit for $n = 0$. Magnetic field, induction and magnetization can be expressed as follows:

Inside the tube:

$$B_\rho(\rho,\varphi) = H_\rho(\rho,\varphi) = 0, \quad B_\varphi(\rho,\varphi) = H_\varphi(\rho,\varphi) = 0; \quad (4)$$

outside of the tube:

$$B_\rho(\rho,\varphi) = H_\rho(\rho,\varphi) = 0, \quad B_\varphi(\rho,\varphi) = H_\varphi(\rho,\varphi) = 0; \quad (5)$$

within the tube walls:

$$m_\rho(\rho,\varphi) = \frac{A}{h_\rho \rho}, \quad m_\varphi(\rho,\varphi) = \frac{-iA}{h_\rho \rho}\sqrt{1+\frac{\omega_M}{\omega_H}}, \quad (6)$$

$$H_\rho(\rho,\varphi) = \frac{-4\pi A}{h_\rho \rho}, \quad H_\varphi(\rho,\varphi) = 0, \quad (7)$$

$$B_\rho(\rho,\varphi) = 0, \quad B_\varphi(\rho,\varphi) = \frac{-i4\pi A}{h_\rho \rho}\sqrt{1+\frac{\omega_M}{\omega_H}}, \quad (8)$$

where $h_\rho = \left[(1 - c^2/4\rho^2)^2 + (c^2/\rho^2)\sin^2\varphi\right]^{1/2}$, and $(\rho,\ \varphi)$ are the elliptic cylindrical coordinates.

For $n = 0$ the resonant frequency field dependence is given by

$$\omega_0 = \gamma\sqrt{H(H+4\pi M)}, \quad (9)$$

which is the same as the expression for the ferromagnetic resonance (FMR) of an infinite film.

The $n = 0$ mode has the following features that can be seen by exploring expressions (8) and (9). The mode frequency does not depend on the tube dimensions. That supports the good fit of the experimentally measured $n = 0$ mode despite the distortions in the tube shape. Amplitude of the magnetization oscillation, m, is maximal on the inner surface of the tube and decays toward the outer surface; therefore this mode is a feature of the tube geometry; in ferromagnetic wires the $n = 0$ mode will be a volume, not surface mode.[34] The magnetization precession is elliptical and the ellipticity is not dependent on the position within the tube walls but is defined by the ratio of tube saturation magnetization and external magnetic field:

$$m_\rho(\rho,\varphi)/m_\varphi(\rho,\varphi) = \frac{i}{\sqrt{1+\frac{\omega_M}{\omega_H}}}. \quad (10)$$

Magnetic field and magnetic induction vectors are orthogonal within the tube walls. m is maximal when pointing along the tube perimeter and couples well to the h produced by the high frequency currents in the exciting wire that short circuits the end of the coplanar waveguide. Due to the ellipticity of the magnetization precession and the alignment of the ellipse major semiaxis along the tube perimeter the magnetic moments precess mostly in the plane of the tube surface and do not generate magnetic fields outside of the tube. This makes the $n = 0$ mode immune to the tube surrounding.

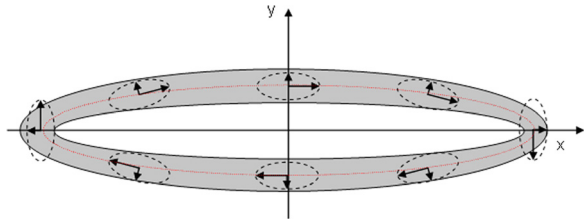

FIG. 6. (Color online) Schematic of the $n = 0$ mode of magnetostatic spin oscillations in elliptical tube.

In FMR all magnetic moments of the film are precessing in phase. If one thinks of our tubes as of a folded infinite ferromagnetic film with periodic boundary conditions magnetic moments of the opposite walls of the tube will oscillate 180 degrees out of phase as schematically shown in Fig. 6. As one can see the lowest frequency mode with $n = 0$ *is not a FMR of the tube but a resonance in which the magnetic moments oscillate in phase along the perimeter of the tube*.

The higher frequency (outer) mode with $n = 1$ represents a spin wave with wavelength equal to the tube perimeter where $m = 0$ at the extremal points on the long axis of the ellipse. For this mode all magnetic moments of the tube oscillate in phase and therefore this mode is most like the FMR of the tube and probably is the mode seen in experiments by Mendach *et al.*[28]

Although the fabricated tube has a topology of an elliptical tube it is obvious, from the cross section shown in Fig. 5 that the tube's profile is not at all elliptical but has gross distortions where the CoTaZr film goes over the coupling loops. Mode indices for the model elliptical tube are probably not useful here. We may assume that the irregular shape will allow coupling to nearly all modes albeit with differing strengths. The highest frequency peak observed in our experiments coincides with the top of the magnetostatic magnetization oscillation band in an elliptical tube ($n \to \infty$) which also coincides with a top of the magnetostatic surface spin wave band of an infinite slab and can be written as: $\omega_\infty = \gamma(H + 4\pi M/2)$. As $n \to \infty$ the spin wave length becomes very short in comparison to the tube wall-to-wall distances and despite the distortions from the elliptical shape the tube behaves as a ferromagnetic film folded into a tube and supports magnetostatic surface waves circulating along the tube perimeter. As in the infinite slab, at large k-vectors, the spin wave outer and inner modes become degenerate; the confluence of the many modes with large wave vectors to a single frequency results in a well defined peak at the top of the spectrum as observed and shown in Fig. 2.

This observation suggests an alternative model that is more intuitive. We compare magnetostatic surface spin wave modes in an infinite ferromagnetic film[35] with periodic boundary conditions that match the tube perimeter with the experimental data. Exchange interaction was not taken into account. The tube profile was approximated by a 200 nm thick ferromagnetic film folded into tube with perimeters equal 12 and 8 μm, respectively, which correspond to the inner and outer perimeters of the fabricated structure. Results of this approximation for the first 12 modes and $n \to \infty$ mode are shown as lines in Fig. 4(b). The modes with $n = 0$

and $n \to \infty$ fit the experimental data for lowest and highest frequency peaks very well. These modes that provide a lower and upper bound on the band of spin excitations do not depend on the perimeter of the tube since either all spins are oscillating in-phase ($n = 0$) or the spin wave wavelength is small in comparison to the tube perimeter ($n \to \infty$). Of course the contorted shape of the experimental "tubes" precludes indexing the intermediate frequency peaks as it did for the more rigorous model based on the elliptic tube.

IV. SUMMARY

In summary, we have measured microwave transmission through lithographically fabricated coplanar waveguides coupled by novel ferromagnetic tubes with distorted profile. Experimental data was compared with a model calculation of magnetostatic surface oscillations in an infinitely long elliptical ferromagnetic tube as well as with surface spin waves in an infinite ferromagnetic film with periodic boundary conditions. While we expect to observe no clear mode indexing due to the irregular shape of the tube, the frequency band of the observed modes agrees with the predictions of an elliptical tube and coincides with the spectral bandwidth of magnetostatic surface waves of an infinite slab. We do recognize that the lowest frequency mode has the largest amplitude because the in-phase oscillation of the magnetization along the tube perimeter coincides with the direction of the exciting magnetic fields. A well defined high frequency limit develops as the circumferential surface wave lengths become small compared to the dimensions of the tube and asymptotically approach the short wavelength high frequency limit of the infinite slab. Between these limits, the irregular shape allows us couple to various modes, the strength of which is probably controlled by the details of the shape.

The fabricated structures are potentially important as high frequency tunable filters. As interesting as the surface modes are, the strong $n = 0$ mode is probably the most useful. In order to make the filter work efficiently the input inductance of the filter should be increased either by increasing the number of exciting wires inside the magnetic tube (winding) or more conveniently by increasing the tube length while keeping other dimensions the same. Lengthening the tubes should introduce strong shape anisotropy. The ground state will have the magnetization along the tube without external bias and a strong resonance transmission at $H = 0$. Resonance could be fine tuned by "on circuit board" fields and or self-fields produced by DC currents flowing in the wires encased by the tubes.

ACKNOWLEDGMENTS

This work is supported by NERC via the Nanoelectronics Research Initiative (NRI), by Intel Corp. and UC Discovery at the Western Institute of Nanoelectronics (WIN) Center. The authors would like to thank A. N. Cleland for the use of the vector network analyzer and hosting aspects of this work in his laboratory. The authors are also thankful to the staff of the UCSB ECE nanofabrication facilities, especially to Brian Thibeault, for helpful discussions of the fabrication processes.

[1]B. Kuanr, Z. Celinski, and R. E. Calmey, Appl. Phys. Lett. **83**, 3969 (2003).
[2]A. M. Crawford, D. Gardner, and S. X. Wang, IEEE Trans. Magn. **38**, 3168 (2002).
[3]D. S. Gardner, G. Schrom, P. Hazucha, F. Paillet, T. Karnik, S. Borkar, J. Saulters, J. Owens, and J. Wetzel, IEEE Trans. Magn. **43**, 2615 (2007).
[4]A review: D. A. Allwood, G. Xiong, C. C. Faulkner, D. Atkinson, D. Petit, and R. P. Cowburn, Science **309**, 1688 (2005).
[5]W. A. Roshen and D. E. Turcotte, IEEE Trans. Magn. **24**, 3213 (1988).
[6]T. Schneider, A. A. Serga, B. Leven, B. Hillebrands, R. L. Stamps, and M. P. Kostylev, Appl. Phys. Lett. **92**, 022505 (2008).
[7]M. Kostylev, A. A. Serga, T. Schneider, B. Leven, and B. Hillebrands, Appl. Phys. Lett. **87**, 15 (2005).
[8]A. Khitun, M. Bao, and K. L. Wang, IEEE Trans. Magn. **44**, 2141 (2008).
[9]A review: J. D. Adam, L. E. Davis, G. F. Dionne, E. F. Schloemann, and S. N. Stitzer, IEEE Trans. Microwave Theory Tech. **50**, 721 (2002).
[10]B. Kuanr, I. R. Harward, D. L. Marvin, T. Fal, R. E. Camley, D. L. Mills, and Z. Celinski, IEEE Trans. Magn. **41**, 3538 (2005).
[11]J. Jorzick, S. O. Demokritov, C. Mathieu, B. Hillebrands, B. Bartenlian, C. Chappert, F. Rousseaux, and A. N. Slavin, Phys. Rev. B **60**, 15194 (1999).
[12]A. Kozhanov, D. Ouellette, Z. Griffith, M. Rodwell, A. P. Jacob, D. W. Lee, S. X. Wang, and S. J. Allen, Appl. Phys. Lett. **94**, 012505 (2009); A. Kozhanov, D. Ouellette, M. Rodwell, S. J. Allen, D. W. Lee, and S. X. Wang, J. Appl. Phys. **109**, 07D333 (2011).
[13]T. Schneider, A. A. Serga, A. V. Chumak, B. Hillebrands, R. L. Stamps, and M. P. Kostylev, Euro Physics Letters **90**, 27003 (2010).
[14]S. O. Demokritov, A. A. Serga, A. André, V. E. Demidov, M. P. Kostylev, and B. Hillebrands, Phys. Rev. Lett. **93**, 047201 (2004).
[15]U. Hansen, M. Gatzen, V. E. Demidov, and S. O. Demokritov, Phys. Rev. Lett **99**, 127204 (2007).
[16]A. Kozhanov, D. Oeullette, M. Rodwell, S. J. Allen, A. P. Jacob, D. W. Lee, and S. X. Wang, J. Appl. Phys. **105**, 07D311 (2009).
[17]V. Vlaminck and M. Bailleul, Science **322**, 410 (2008).
[18]P. K. Amiri, B. Rajaei, M. Vroubel, and Y. Zhuang, Appl. Phys. Lett. **91**, 062502 (2007).
[19]S. O. Demokritov, V. E. Demidov, O. Dzyapko, G. A. Melkov, A. A. Serga, B. Hillebrands, and A. N. Slavin, Nature Lett. **443**, 430–433 (2006).
[20]V. E. Demidov, J. Jersch, K. Rott, P. Krzysteczko, G. Reiss, and S. O. Demokritov, Phys. Rev. Lett **102**, 177207 (2009).
[21]V. E. Demidov, M. Buchmeier, K. Rott, P. Krzysteczko, J. Münchenberger, G. Reiss, and S. O. Demokritov, Phys. Rev. Lett. **104**, 217203 (2010).
[22]P. Landeros, J. Escrig, D. Altbir, M. Bahiana, and J. d'Albuquerque e Castro, J. Appl. Phys. **100**, 044311 (2006).
[23]J. Lee, D. Suess, T. Schrefl, K. Oh, and J. Fidler, J. Magn. Magn. Mater. **310**, 2445 (2007).
[24]H. Leblond and V. Veerakumar, Phys. Rev. B **70**, 134413 (2004).
[25]T. M. Nguyen and M. G. Cottam, Surf. Sci. **600**, 4151 (2006).
[26]M. A. Popov and I. V. Zavislyak, Ukr. J. Phys. **53**, 702 (2008).
[27]F. S. Li, D. Zhou, T. Wang, L. J. Song, and C. T. Xu, J. Appl. Phys **101**, 014309 (2007).
[28]S. Mendach, J. Podbielski, J. Topp, W. Hansen, and D. Heitmann, Appl. Phys. Lett. **93**, 262501 (2008).
[29]S. O. Demokritov, A. A. Serga, V. E. Demidov, B. Hillebrands, M. P. Kostylev, and B. A. Kalinikos, Nature **426**, 159 (2003).
[30]F. Balhorn, S. Mansfeld, A. Krohn, J. Topp, W. Hansen, D. Heitmann, and S. Mendach, Phys. Rev. Lett. **104**, 037205 (2010).
[31]K. Hayashi, M. Hayakawa, Y. Ochiai, H. Matsuda, W. Ishikawa, Y. Iwasaki, and K. Aso, J. Appl. Phys. **61**, 2983 (1987).
[32]D. W. Lee and S. X. Wang, J. Appl. Phys. **103**, 07E907 (2008).
[33]M. R. Scheinfein and E. A. Price, *LLG Micromagnetic Simulator*™, http://llgmicro.home.mindspring.com/.
[34]I. Joseph and E. Schlomann, J. Appl. Phys. **32**, 1001 (1961).
[35]R. W. Damon and J. R. Eshbach, J. Phys. Chem. Solids **19**, 308 (1961).